Multi-Objective Optimization for a Dual-Flux-Modulator Coaxial Magnetic Gear with Double-Layer Permanent Magnet Inner Rotor

Liu, Xiao; Zhao, Yunyun; Lu, Meng; Chen, Zhe; Huang, Shoudao

Published in:
IEEE Transactions on Magnetics

DOI (link to publication from Publisher):
10.1109/TMAG.2021.3065464

Publication date:
2021

Document Version
Accepted author manuscript, peer reviewed version

Multi-objective Optimization for a Dual-Flux-Modulator Coaxial Magnetic Gear with Double-Layer Permanent Magnet Inner Rotor

Xiao Liu[1], Yunyun Zhao[1], Meng Lu[1], Zhe Chen[2], and Shoudao Huang[1]

[1] Hunan University, College of Electrical and Information Engineering, Changsha, China
[2] Aalborg University, Department of Energy Technology, Aalborg East, Denmark

In order to improve the torque capability and permanent magnets (PMs) utilization efficiency of the dual-flux-modulator coaxial magnetic gear (DFM-CMG), a double-layer PMs (DLPM) layout on the inner rotor (IR) is proposed. In this paper, the torque performance of the DFM-CMG is investigated by 3-D finite element analysis and validated by corresponding experiment. According to parametric analysis results, it is found that six dimensional design parameters can significantly affect the stall torque (ST) and ST per PM volume (STPPV) of the DFM-CMG. To achieve multi-objective optimization (MOO) of the DFM-CMG given that the ST and STPPV normally conflict with each other, a metamodel-based MOO method is employed under the premise of the constant active region volume. The optimized DFM-CMG with DLPM IR shows a 19.7% and 2.2% growth in the STPPV than the initial design and the optimized counterpart with single-layer PMs IR under the same constraint of the ST. Furthermore, the optimized DFM-CMG with DLPM IR possesses excellent PMs utilization efficiency compared to other typical CMGs.

***Index Terms*—Dual-flux-modulator coaxial magnetic gear (DFM-CMG), double-layer permanent magnets (PMs) layout, metamodel-based multi-objective optimization (MOO), PMs utilization efficiency, torque capability.**

I. Introduction

Coaxial magnetic gears (CMGs) are promising candidates for power transmission, which could realize non-contact torque and speed operation with the help of flux modulation effect [1]. The CMGs have attracted great attentions in recent years due to the excellent transmission properties of minimum friction loss, low acoustic noise and overloads self-protection. A dual-flux-modulator coaxial magnetic gear (DFM-CMG) was proposed and studied in [2], which showed better torque characteristics comparing to other types of CMG. However, it is still possible to further improve the torque performance of the DFM-CMG by optimization. Besides, it has been proven that the multilayer permanent magnets (PMs) rotor layout has the advantages of lower flux leakage, higher rotor saliency and specific reluctance torque production, comparing to the single-layer PMs (SLPM) rotor [3]. In this paper, a double-layer PMs (DLPM) layout is adopted in the inner rotor (IR) of a DFM-CMG for suppressing the flux leakages and improving the torque performance. In addition, the torque capability of PMs devices exhibits a strong correlation with the consumption of PMs [4]. The PMs usage ratio should be paid more attention for the CMGs, due to the massive consumption of PMs. Therefore, it is very essential to perform the multi-objective optimization (MOO) design for DFM-CMG with DLPM IR aiming to maximize the ST and ST per PM volume (STPPV) simultaneously.

In this study, the 3D finite element (FE) model of the DFM-CMG is developed and validated by corresponding experiment. Furthermore, the effects of the design parameters of PMs and auxiliary flux modulator (AFM) on the ST and STPPV are investigated. Finally, MOO design of DFM-CMG with DLPM IR is implemented by applying a multi-objective method with polynomial regression (PR) metamodels and multi-objective particle swarm optimization (MOPSO) algorithm [7].

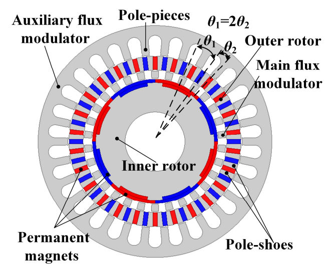

Fig. 1. Configuration of the DFM-CMG with DLPM IR.

TABLE I
Key Parameters of the DFM-CMG

Parameters	Value (unit)
Number of pole-pairs for the IR (p_{IR})	4
Number of pole-pairs for the OR (p_{OR})	26
Theoretical gear ratio	6.5
Number of main modulation pole-pieces (N_m)	30
Number of AFM teeth (N_{AFM})	30
PMs total thickness of IR (t_{IR})	6 mm
Pole-arc coefficient of IR (α_p)	1
Ratio of inner and outer layer PM angle (α_R)	1
PMs width of OR (w_{OR})	5 mm
PMs length of OR (l_{OR})	15 mm
Teeth length of AFM (l_T)	21 mm
Yoke length of AFM (l_Y)	12 mm
Teeth angle of AFM (θ_T)	5°
Air-gap length	1 mm
Stack length	60 mm
Remanence of PMs	1.23 T

II. Numerical simulation of the DFM-CMG

A. Topology Configuration and FE Modeling

Fig. 1 shows the configuration of the DFM-CMG. The key parameters of the DFM-CMG are listed in Table I. The DFM-CMG employs surface-mounted PMs for the IR but spoke-type PMs for the outer rotor (OR). Different from the conventional DFM-CMG with SLPM IR, a DLPM layout on the IR with no gap between two layers of PMs is introduced for the proposed novel DFM-CMG. The main modulation ring (MMR) is sandwiched between the two rotors. The MMR would couple the modulated magnetic fields in the two air-gaps, when the corresponding relationship is satisfied [1]

$$p_{\mathrm{IR}} + p_{\mathrm{OR}} = N_{\mathrm{m}} \quad (1)$$

A stationary AFM is placed on the outermost layer. In order to achieve the magnetic-gearing effect as the MMR, the following relationship needs to be obeyed,

$$N_{\mathrm{AFM}} = N_{\mathrm{m}} \quad (2)$$

In addition, to enhance the magnetic gearing effect, the pitch angle of the pole-pieces on MMR θ_1, and angle difference between the axis of pole piece on AFM and neighboring pole piece on MMR θ_2 satisfy [2]

$$\theta_1 = 2\theta_2 \quad (3)$$

Then, a FE model of the DFM-CMG is developed and solved by using 3-D Maxwell software.

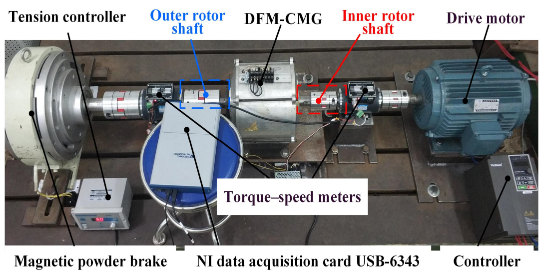

Fig. 2. Test rig of existing DFM-CMG.

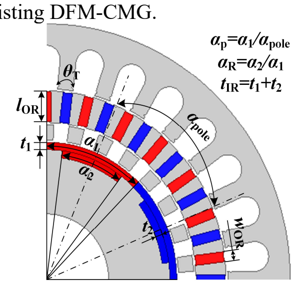

Fig. 3. The design parameters of the DFM-CMG with DLPM IR.

B. Validation of the FE Model

A test rig for the torque performance measurement of the existing conventional DFM-CMG is shown in Fig. 2. The OR of measured DFM-CMG is loaded by a magnetic powder brake, while the IR is rotated by a driving motor. Two torque-speed meters are used to measure the torques and speeds of the two rotors, and the torque-speed signals are collected by a NI data acquisition card USB-6343. Because the accuracy of the FEM simulation results may affect the accuracy of the metamodels directly and further affect reliability of the optimization, it is more reasonable to use the 3D FEM at the expense of calculation time. In order to validate the 3-D FE simulation models of DFM-CMG, the simulation results are compared with the experimental data under the static load. The tested ST on the OR is 190.0 Nm, which is very close to the 3-D FE simulation result of 194.2 Nm. As the relative error between the simulation and experimental results is only 2.21%, the accuracy of the 3D FE model is validated. The trade-off made on the manufacturing and assembling of the DFM-CMG accounts for the tiny discrepancies probably. The same FE modeling method is adopted for the proposed DLPM DFM-CMG in the later sections, and the FE simulation models and results are feasible to be used for further study.

III. Parametric Analysis

It has been proved that the torque performance of CMGs may exhibit a strong correlation with several parameters [5]. Eight dimensional parameters, *i.e.*, t_{IR}, α_{p}, α_{R}, w_{OR}, l_{OR}, l_{T}, l_{Y} and θ_{T} are considered as the design parameters to be investigated, as shown in Fig. 3. t_1 and t_2 are the outer and inner layer PMs thickness on the IR, respectively, with no gap between the above two layers PMs. α_1 and α_2 are the pole arc lengths of the outer and inner layer PMs on the IR, respectively. α_{pole} is the polar distance of IR. The other unstudied design parameters are kept as the initial design.

A. Effect of the IR PMs Dimensions

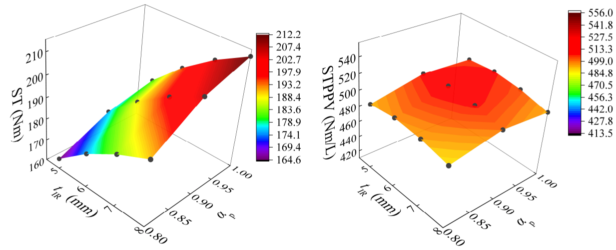

(a) (b)

Fig. 4. The effect of t_{IR} and α_{p} on torque performance. (a) ST. (b) STPPV.

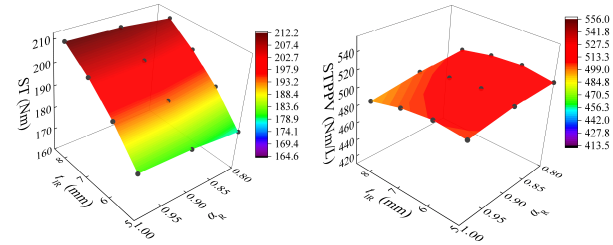

(a) (b)

Fig. 5. The effect of t_{IR} and α_{R} on torque performance. (a) ST. (b) STPPV.

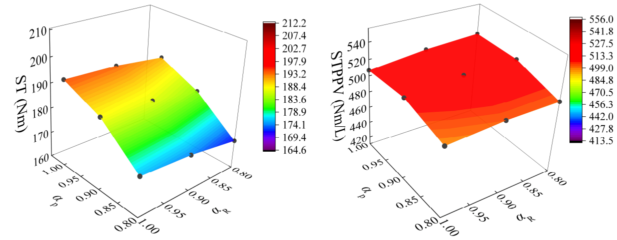

(a) (b)

Fig. 6. The effect of α_{p} and α_{R} on torque performance. (a) ST. (b) STPPV.

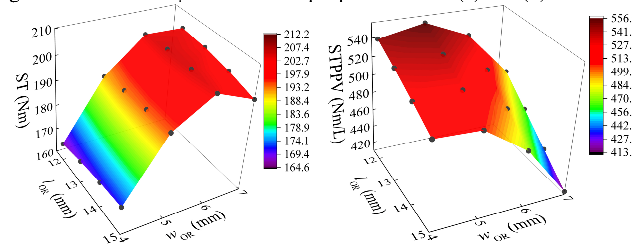

(a) (b)

Fig. 7. The effect of l_{OR} and w_{OR} on torque performance. (a) ST. (b) STPPV.

Figs. 4-6 show the effect of IR dimensions t_{IR}, α_{p} and α_{R} singly on the ST and STPPV of the DFM-CMG with DLPM IR, while other parameters remain unchanged. Although the ST is going up with the growth of all three dimensions t_{IR}, α_{p} and α_{R}, t_{IR} and α_{p} have a greater effect on the ST than the α_{R}. It could be noticed that increasing the IR PMs consumption will definitely benefit the ST. It is also found that the STPPV

This article has been accepted for publication in a future issue of this journal, but has not been fully edited. Content may change prior to final publication. Citation information: DOI 10.1109/TMAG.2021.3065464, IEEE Transactions on Magnetics

generally first increases, and then decreases with the raise of t_{IR}, α_p and α_R due to the magnetic saturation of PMs and steel laminations.

B. Effect of the OR PMs Dimensions

The evolution of the ST and STTPV as a function of l_{OR} and w_{OR} changing within 12-15 mm and 4-7 mm respectively are shown in Fig. 7, while fixing the other parameters. It can be found from Fig. 7 (a) that ST first rapidly raises and then slightly decreases with the increase of w_{OR}. It is interesting to note from Fig. 7 (b) that as w_{OR} increases, the STPPV does not monotonously change. It is also found that the STPPV decreases with the growth of l_{OR}. It is because the ST is not very sensitive to the change of l_{OR} , but the usage of PMs obviously rises with the growth of l_{OR}. Hence, it could be concluded that the OR PMs dimensions have an important and complex effect on the STPPV.

C. Effect of the AFM Dimensions

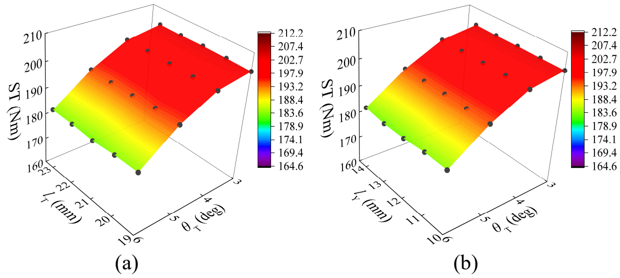

Fig. 8. The effect on ST. (a) l_T and θ_T. (b) l_Y and θ_T.

Fig. 8 (a) and (b) present the 3-D trend profiles of ST with different values of l_T, θ_T and l_Y, θ_T, respectively. The ST would decrease with the increase of the θ_T and the highest ST could be achieved at θ_T =3°, as shown in Fig. 8. However, the ST hardly changes with the variation of l_T and l_Y. As the parameters of the θ_T, l_T and l_Y are independent of the PMs consumption, the variation trend of the STPPV with these parameters would be the same as that shown in Fig. 8.

Based on the parametric analysis and discussion, six design parameters i.e. t_{IR}, α_p, α_R, w_{OR}, l_{OR} and θ_T, are found to have a strong effect on the ST and STPPV of studied DFM-CMG, which is worthy of being further optimized.

IV. MOO Design of the DFM-CMGs

A. Optimization Method

The impact of the design parameters of PMs and AFM on torque performance has been explored in section III. However, parametric analysis could not find the global optimal designs. In order to simultaneously maximize the ST and STPPV, the MOO designs for the DFM-CMG with DLPM IR are carried out. Typically, the MOO problem could be formulated as (4), while the unstudied parameters are kept as the initial design.

TABLE II
Accuracies Assessment of the Metamodels

	RMSEN	R^2	MEN
ST	0.0163	0.9964	0.0318
STPPV	0.0172	0.9959	0.0339

$$\begin{cases} \min & \text{-ST, -STPPV} \\ s.t. & 5\text{ mm} \le t_{IR} \le 8\text{ mm} \\ & 0.8 \le \alpha_p \le 1.0 \\ & 0.8 \le \alpha_R \le 1.0 \\ & 4\text{ mm} \le w_{OR} \le 7\text{ mm} \\ & 12\text{ mm} \le l_{OR} \le 15\text{ mm} \\ & 3^\circ \le \theta_T \le 6^\circ \end{cases} \tag{4}$$

Due to the high dimensionality and complexity of the DFM-CMG with two rotors and two flux modulators, it is difficult to optimize the DFM-CMG by using conventional analytical optimization method. The mathematical procedures assisted with metamodels have been widely used in the design of the modern electrical machines [4], in which the coupling of several design parameters would be taken into the account. A metamodel-based MOO method is employed in this study, and the flow chart of the method is shown in Fig. 9. The full factorial design method, which is one of typical design of experiments (DOEs), is adopted to generate 324 sampling points totally due to the advantage of its uniformity.

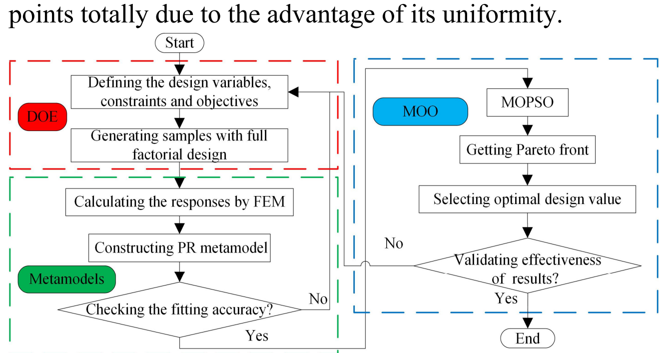

Fig. 9. Flow chart of the MOO.

The ST and STPPV responses of aforementioned sample points are obtained by 3D FEM. Based on these design samples, the PR metamodels are developed to calculate the values of the ST and STPPV. The normalized root mean square error (RMSE), square value (R^2) and normalized maximum error (ME) are used to assess the accuracies of the metamodels, which can be written as

$$\text{RMSE} = \frac{\sqrt{\dfrac{\sum_{k=1}^{n}\left(y_k - \hat{y}_k\right)^2}{n}}}{y_{k\_\max} - y_{k\_\min}} \tag{5}$$

$$R^2 = 1 - \sum_{k=1}^{n}\left(y_k - \hat{y}_k\right)^2 \Big/ \sum_{k=1}^{n}\left(y_k - \bar{y}_k\right)^2 \tag{6}$$

$$\text{ME} = \left(\frac{\max\left|y_k - \hat{y}_k\right|}{y_{k\_\max} - y_{k\_\min}}\right),\ k = 1, 2, \ldots, n \tag{7}$$

where n denotes the number of new accuracy assessment sample points. y_k and $\hat{y}_k$ are the response values calculated by FEM and the corresponding predicted values calculated by metamodels for error accuracy assessment point k, and $\bar{y}_k$ represents the mean of the y_k . Generally, the smaller RMSE and ME are better, and the R^2 closer to 1 indicates higher accuracy for the PR metamodels. The results of error analysis for PR metamodels are listed in Table II. It can be found that all the R^2 are close to 1, which means the PR metamodels are accurate enough to predict the responses of ST and STPPV. Thus, the metamodels above would be adopted in the following MOO. Finally, the MOPSO is employed to simultaneously maximize the ST and STPPV while keeping the active region volume constant.

B. Optimization Results

The MOO for both conventional and novel DFM-CMGs are implemented. Fig. 10 compares the Pareto fronts for the DFM-CMGs with SLPM and DLPM layout. The STPPV of the optimized point O_2 has a 2.2% growth than that of optimized point O_1 under the same constraint of ST. Compared with the initial design point I, the optimal design O_2 has a 19.7% growth in STPPV on condition of the same ST level. The optimums at right side of point O_1 and O_2, in the black-dotted area as shown in Fig. 10, could simultaneously increase the ST and STPPV comparing to the initial design. The optimization results of dimensional design parameters at the point O_1 and O_2 are listed in Table III. Consequently, the ST and STPPV of the above optimum designs are calculated by FEM. As shown in Table III, it could be found that these errors between the FE simulation results and the optimization results obtained by metamodels are lower than 0.05%, indicating the effectiveness of the metamodel-based MOO method. According to various design requirements, a set of optimal designs could be picked up from Pareto fronts shown in Fig. 10 (a). Furthermore, it is also found that the green Pareto fronts as shown in Fig. 10(a) all locate to the top right of those red solutions, indicating that the DLPM IR layout could present better Pareto fronts than the SLPM counterparts. Therefore, it is proved that the DFM-CMG with DLPM layout on the IR could improve the ST and STPPV simultaneously.

TABLE III
COMPARISON OF OPTIMUM DESIGNS FOR THE DFM-CMGS

		Optimal value (SLPM IR layout)	Optimal value (DLPM IR layout)
Design parameters	t_{IR}	6.05 mm	6.24 mm
	α_p	0.92	0.95
	α_R	1	0.81
	w_{OR}	4.83 mm	4.81 mm
	l_{OR}	12.00 mm	12.00 mm
	θ_T	3.00°	3.02°
ST	Metamodel	194.43 Nm	194.54 Nm
	FEM (3D)	194.50 Nm	194.62 Nm
	Error	0.04%	0.04%
STPPV	Metamodel	593.77 Nm/L	606. 95 Nm/L
	FEM (3D)	593.93 Nm/L	606. 73 Nm/L
	Error	0.03%	0.04%

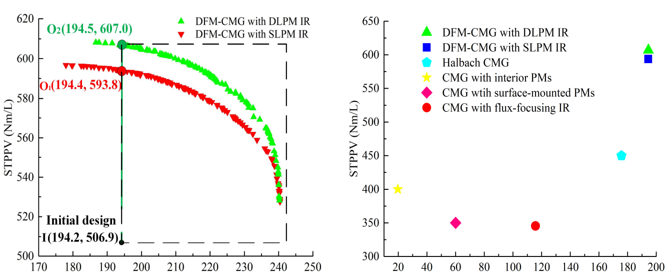

(a) (b)

Fig. 10. (a) Comparison of Pareto fronts for DFM-CMGs with SLPM and DLPM. (b) Comparison of STPPV both DFM-CMGs and other typical CMGs [6].

In addition, according to the study in [6], Fig. 10 (b) compares the STPPV calculated by FEM of the DFM-CMGs and that of other typical CMGs. It could be seen that the DFM-CMGs are superior in terms of the STPPV as well as torque capability among four types of typical CMGs. Moreover, it is worth noting that the DFM-CMG with DLPM IR studied in this paper has the highest STPPV, up to 608 Nm/L, which is much higher compared with that of other typical CMGs. As a result, the DFM-CMG with DLPM IR layout is believed to be a promising power transmission device in future industrial applications as it possesses the best PMs usage ratio and torque capability.

V. CONCLUSIONS

In this paper, a DFM-CMG with DLPM IR is proposed, and the torque performance of the DFM-CMG is investigated by FEM. According to the parametric analysis, six dimensional parameters of the DFM-CMG are found to have significant effects on the ST and STPPV. The metamodel-based MOO method is employed to maximize the ST and STPPV simultaneously. The optimized DFM-CMG with DLPM IR shows a 19.7% and 2.2% growth in the STPPV than the existing initial design and the optimized counterpart with SLPM IR under the same constraint of the ST, which demonstrates that the proposed optimization approach can significantly improve the torque performance of DFM-CMGs. Furthermore, it could be found that the PMs usage ratio of novel DFM-CMG with DLPM IR is much higher than other typical CMGs. As a result, the DFM-CMG with DLPM IR would be a potential power transmission device in future industrial applications.

ACKNOWLEDGMENT

This work was supported by the National Natural Science Foundation of China (Grant No. 51877074) and the Natural Science Foundation of Hunan Province, China (Grant No. 2020JJ2005).

REFERENCES

[1] K. Atallah and D. Howe, “A novel high-performance magnetic gear,” *IEEE Trans. Magn.,* vol. 37, no. 4, pp. 2844-2846, Jul. 2001.
[2] X. Zhang, X. Liu, and Z. Chen, “A novel dual-flux-modulator coaxial magnetic gear for high torque capability,” *IEEE Trans. Energy Convers.,* vol. 33, no. 2, pp. 682–691, Jun. 2018.
[3] X. Zhu, S. Yang, Y. Du, Z. Xiang, and L. Xu, “Electromagnetic performance analysis and verification of a new flux-intensifying permanent magnet brushless motor with two-layer segmented permanent magnets,” *IEEE Trans. Magn.,* vol. 52, no. 7, Jul. 2016, Art. no. 8204004.
[4] G. Bramerdorfer, J. A. Tapia, J. J. Pyrhönen, and A. Cavagnino, “Modern electrical machine design optimization: Techniques, trends, and best practices,” *IEEE Trans. Ind. Electron.*, vol. 65, no. 10, pp. 7672–7684, Oct. 2018.
[5] M. Filippini and P. Alotto, “Coaxial magnetic gear design and optimization,” *IEEE Trans. Ind. Electron.,* vol. 64, no. 12, pp. 9934–9942, Dec. 2017.
[6] Y. Wang, M. Filippini, N. Bianchi and P. Alotto, “A review on magnetic gears: topologies, computational models and design aspects,” *IEEE Trans. Ind. Appl.*, vol. 55, no. 5, pp. 4557-4566, Sept.-Oct. 2019.
[7] C. Coello, G. Pulido, and M. Lechuga, “Handling multiple objectives with particle swarm optimization,” IEEE Trans. Evol. Comput., vol. 8, no. 3, pp. 256–279, Jun. 2004.